

Far-Field Optical Nanoscopy

Stefan W. Hell

Summary. Since the discovery of the diffraction barrier in the nineteenth century, it has been commonly accepted that a lens-based (far-field) optical microscope cannot discern structural details much finer than about half the wavelength of light ($\lambda/2$). However, in the early 1990s, a quest toward higher resolution began, which led to the discovery that the diffraction barrier of far-field fluorescence microscopy can be radically overcome using basic molecular transitions. This chapter discusses the initial and more recent concepts that can provide far-field optical resolution down to the molecular scale. It is shown that all concepts reported and implemented to date exploit a transition between a bright and a dark state to switch the fluorescence capability of molecules such that adjacent objects or molecules emit sequentially in time. Some of these concepts can be extended to signal-giving mechanisms other than fluorescence. Likewise, purely transition-based concepts, such as stimulated emission depletion (STED) microscopy, can in principle be extended to explore the molecule itself. Emergent far-field fluorescence nanoscopy will impact not only the life sciences but also other areas that benefit from nanoscale three-dimensional (3D) mapping with conventional lenses and propagating light.

19.1 Introduction and Overview

By providing a spatial resolution down to the atomic scale, electron and scanning probe microscopy have revolutionized our understanding of life and matter. Nonetheless, optical microscopy has maintained its key role in many fields, in particular in the life sciences. This stems from a number of rather exclusive advantages, such as the noninvasive access to the interior of (living) cells and the specific and highly sensitive detection of cellular constituents through fluorescence tagging. As a matter of fact, lens-based fluorescence microscopy would be almost ideal for investigating the three-dimensional (3D) cellular interior if it could resolve details far below the wavelength of light. However, until not very long ago, obtaining a spatial resolution on the nanometer scale with an optical microscope that uses lenses and focused visible light was considered unfeasible [1, 2].

Focusing a propagating light wave means causing it to interfere constructively at a certain point in space, called the geometrical focal point $(0,0,0)$. Due to diffraction a focal intensity pattern $I(x, y, z)$ emerges around $(0,0,0)$, which is also referred to as the intensity point-spread-function (PSF) of the lens. $I(x, y, z)$ features a central maximum called the focal spot (Fig. 19.1a) whose full-width-half-maximum (FWHM) is $\Delta r \approx \lambda/(2n \sin \alpha)$ in the focal plane and $\Delta z \approx \lambda/(n \sin^2 \alpha)$ along the optic axis [3]. λ is the wavelength of light, α denotes the semi-aperture angle of the lens, and n is the refractive index of the object medium (Fig. 19.1a). Discerning similar objects lying within this spot is usually precluded because they are illuminated in parallel and hence give off (fluorescence) photons in parallel. Likewise, the propagation of the emitted (fluorescence) light that is collected by a lens and focused to an image plane is governed by a similar function $I_{\text{em}}(x, y, z)$, describing the blur of the coordinate from where the photons originated.

A logical consequence of the fact that light cannot be focused more sharply than the diffraction limit was to give up propagating waves and lenses and confine the light by means of a subdiffraction-sized aperture or tip. Placing this aperture in sub- $\lambda/2$ proximity to the object and scanning it across the object renders optical images with subdiffraction resolution. Proposed by Synge [4] in 1928 and again by Ash and Nicholls in 1972 [5], this concept was invigorated in the wake of the invention of the scanning tunneling microscope as near-field optical microscopy [6, 7]. A fundamental difference of near-field optical microscopy to its lens-based (far-field) counterpart is that it relies on non-propagating, evanescent light fields fading out exponentially within distance $\sim \lambda/2$ from the object. Giving up focusing therefore comes at a high price: one is bound to imaging surfaces.

Because it also relies on collecting and amplifying evanescent waves, the same practical limitation applies to the recently introduced lens of negative refractive index [8]. In its currently most sophisticated version, called hyperlens [9,10], the evanescent waves are converted into propagating waves forming a magnified image of the sample on a distant screen, which is why one may think that it is far-field imaging. However, the projection to a distant screen does not change the fact that the hyperlens relies on the sample's near-field. Hence, in its current state of development, a hyperlens is not a far-field imaging device [11], but a fascinating non-scanning concept of employing the near-field.

In the twentieth century, several ideas have been put forth to address the resolution problem in the far-field as well. For example, in 1956, Toraldo di Francia suggested shrinking the central focal spot by applying an elaborate phase pattern in the entrance pupil of the objective lens [12]. Unfortunately, the creation of smaller central spots is accompanied with giant sidelobes rendering this concept impractical. In 1966, Lukosz [13] suggested that the use of gratings for the illumination and/or the detection pathway should improve the resolution in reflection imaging, but this concept yields a factor of two at most [5]. While he suggested that the resolution can be improved by reducing the microscope's field of view (which is also inherent in Synge's near-field idea),

no concrete indication was given as to how a reduction by more than 2-fold could be realized with focused light. In 1978, it was speculated that a hypothetical elliptic “ 4π point hologram” would be able to focus light waves to a subdiffraction-sized spot or simply to a point, thus overcoming the diffraction

Fig. 19.1 (Continued). By ensuring that the doughnut intensity I exceeds I_s in a large area, the spot (*green*) in which the fluorophore can still be bright and active is confined to subdiffraction dimensions. Here, a measured 20-nm diameter spot is shown, which is approximately ten times below the diffraction barrier. Scanning such a subdiffraction sized spot across the sample yields subdiffraction images. (d) The concepts STED, GSD, (left-hand side) and SPEM/SSIM (right-hand side) can be viewed as special cases of a more general concept called RESOLFT. A hallmark of this generalized concept is that it utilizes focal light distributions $I(r)$ with zero-intensity points at positions r_i , to confine either a bright (A) or a dark fluorophore state (B) in space. The zeros are preferably $> \lambda/(2n)$ apart in the focal plane. Two examples of this generalized concept are shown. *Left*: the intensity drives a transition $A \rightarrow B$ to confine the *bright* state A in space. This is the case for a parallelized STED, GSD, or a RESOLFT approach using reversibly photoactivatable proteins or photochromic dyes. *Right*: in the SPEM/SSIM concept the intensity $I(r)$ drives a transition $B \rightarrow A$ that confines the *dark* state B in space. In both cases, the positions of state A or B are predefined in space by $I(r)$ and r_i . When imaged onto a camera the steep regions of state A (*left*) or state B (*right*) become blurred. However, the diffraction blur can be dealt with (as shown in the left-hand panel STED, GSD) by allocating the signal (from the diffraction blob) to the known coordinate r_i of the zero in the sample space. The image is gained by scanning the array of zeros (r_i) across the sample and recording the fluorescence for each step. The diffraction blur can also be dealt with for SPEM/SSIM (right-hand panel) because the superresolved data is encoded in the steeply confined dark regions around r_i of state B . Since SPEM/SSIM initially produces a “negative data set,” the SPEM/SSIM image is finally gained by mathematically converting the negative data set into a positive one. The small boxes in the sketches symbolize the fluorophore molecules that make up the object. $p_A(r) \leq 1$ defines the normalized probability of occurrence of state A . Although all these RESOLFT concepts are suitable to detect single molecules, they generally operate with ensembles. Since the position at which the fluorophores are in A or B and hence emitting is predefined by the zero intensity points r_i , the RESOLFT strategy has also been named the “targeted” read-out mode. (e) The single molecule switching concepts (PALM/STORM) do not define the region where signal is emitted, but read out the fluorophores of the object stochastically, molecule by molecule. Individual fluorophores are sparsely switched to a specific bright state A that is able to emit $m \gg 1$ photons before the molecule returns to B . The detection of $m \gg 1$ photons enables the calculation of the centroid of the diffraction blob of individual molecules when imaged onto a camera. Thus it is possible to assemble an image consisting of centroid tickmarks with a statistically variable resolution depending on m . The concepts (c–e), i.e., STED, GSD, RESOLFT, SPEM/SSIM, and PALM/STORM are not limited by diffraction, meaning that they can resolve similar molecules at nanometer distances

barrier [14]. However, as no near-field component is relayed in this case, a convergence to a subdiffraction spot or even a point is impossible.

Confocal fluorescence microscopy has also been connected with resolution improvement (Fig. 19.1a) [15–17]. Illuminating with a diffraction limited focused spot and detecting with a symmetrically arranged point detector, the effective focal spot, i.e., the effective PSF of this microscope is described by the product of the diffraction pattern for illumination and for detection: $I(x, y, z) I_{\text{em}}(x, y, z) \approx I^2(x, y, z)$. The multiplication of intensities and the nearly quadratic dependence on the intensity in this formula reduces the FWHM of its central spot by $\sim \sqrt{2}$. In the Fourier domain, the multiplication expands the optical bandwidth of spatial frequencies even by a factor of two. In practice, however, $I(x, y, z)$ and $I_{\text{em}}(x, y, z)$ are not really identical and the detector is not point-like [16, 17], meaning that the process is not really quadratic and the limited bandwidth expansion by a factor of two not practically realized. However, even if it were, the newly gained higher frequencies are heavily damped, which is why confocal microscopy did not really provide a higher resolution. Its actual benefit was the improved 3D-imaging and superb background rejection [16, 17].

A genuine quadratic dependence of the measured fluorescence signal on the focal illumination intensity $I(x, y, z)^2$ is provided by (nonlinear) two-photon excitation [18–20]. Exciting a fluorophore from its ground state S_0 to its fluorescent state S_1 requires two photons of half of the difference in energy between the two states, i.e. light of 2λ . The doubling in wavelength means that the size of the diffraction spot of excitation light is also doubled [20], which, unfortunately, is not compensated for by the $\sim \sqrt{2}$ FWHM reduction stemming from the quadratic nonlinearity. As a result, the resolution of a two-photon excitation microscope is usually slightly poorer than its one-photon counterpart, and the spatial frequency bandwidth is not expanded in absolute terms [21]. The same arguments are valid for m -photon absorption processes, because they usually require an even longer wavelength $m\lambda$, let alone the requirement for huge intensities and the low cross-section. However, even if m -fold longer wavelengths were not needed (as is the case for higher order scattering events), as long as m is finite, the resolution barrier is only shifted, not “broken.” “Breaking” implies that the limiting role of diffraction is lifted and that the resolution can be increased, at least conceptually, to the molecular scale or even beyond. Clearly, multiphoton and confocal microscopes do not fulfill this criterion.

Purely mathematical approaches using the PSF of the system and/or a priori object information rarely exceeded a factor of two [17, 22, 23] and were prone to producing artifacts. They can be augmented through additional a priori constraints, such as the objects featuring different absorption or emission spectra [24]. In this case, the resolution problem can become almost trivial, because objects with different spectra can be separated with suitable spectral filters. However, because of the difficulty to mark all features in a sample with different labels, reducing the resolution problem to a color separation

followed by data computation was not an effective pathway either. In my view, the inability of all these superresolution ideas to provide noteworthy improvements cemented the belief of the twentieth century that apart from a factor of two, perhaps, at the end of the day, the resolution of any lens-based light microscope is limited to $\Delta r > 200 \text{ nm} \approx \lambda/2$ and $\Delta z > 450 \text{ nm} \approx \lambda$.

Therefore, until the early 1990s the general belief was that in order to seriously improve the resolution in the visible range one has to discard lenses and resort to near-field optics [25,26]. Consequently, major efforts were undertaken to develop this technique, including for biological imaging [27,28]. While near-field optics became very useful in many areas [29], its restriction to surfaces remained a drawback. At the same time, the importance of lens-based fluorescence microscopy grew, due to the advent of 3D imaging [17] and a myriad of fluorescent markers, including that of the green-fluorescent-protein (GFP) and its derivatives [30,31].

For these reasons, attaining nanoscale resolution with focused light became worthwhile to pursue [32–35]. Moreover, in light of the notion that it was considered impossible, exploring ways to realize nanoscale resolution with regular lenses became a fascinating scientific quest.

The breaking of the diffraction barrier of far-field optical microscopy as we know it today was born out of the insight that the key to far-field nanoscale resolution is held by the fluorophore itself and its interstate transitions [34–36]. This approach was in stark contrast to that of near-field optics which was built on the modification of the propagation of light. The philosophy conveyed in these papers was that there must be transitions in a dye that, when properly implemented in the image formation, should neutralize the limiting role of diffraction [34]. Viewing fluorophores as facilitators of nanoscale far-field optical resolution was a major change in the perception of the fluorophore's role and capability in microscopy, because until then fluorophores were primarily regarded as indicators of molecular species or of physiological parameters such as ion concentrations.

Based on this philosophy, stimulated emission depletion (STED) microscopy [35] and ground state depletion (GSD) microscopy [36] emerged as the first concrete and viable physical concepts to fundamentally overcome the limiting role of diffraction in a lens-based optical microscope. In a nutshell, STED and GSD use a selected pair of bright (fluorescent) and dark fluorophore states to restrict the bright state to subdiffraction dimensions. This is accomplished by resorting to optical transitions that transiently switch off the ability of the dye to fluoresce by confining the dye to a dark state. The transition is effected with a light intensity distribution featuring a zero, switching the fluorescence off everywhere except at zero where the fluorophore is still allowed to be bright. Translating the zero across the specimen switches the signal of adjacent features sequentially on and off, allowing their separate registration. The spatial confinement of molecular states rather than of the light (as in near-field optics) neutralized the limiting role of diffraction in a natural way. Thus, STED and GSD microscopy radically departed from the

superresolution approaches mentioned earlier. They disentangled the wavelength from its resolution-limiting role and suggested that “infinite resolution” [35] was possible without eliminating diffraction per se.

Other proposals to improve *far*-field fluorescence microscopy resolution [21, 37] have followed, which also placed fluorophore transitions at the center stage. Concretely, the concept of STED and GSD microscopy was expanded to photoswitching molecules, specifically of synthetic organic molecules or photoactivatable fluorescent proteins [38–40], in an approach dubbed RESOLFT [41, 42], standing for reversible saturable/switchable optical linear (fluorescence) transitions. A hallmark of all these concepts is that they yield images without mathematical processing and without any assumptions about the object or the performance of the lens. They are purely “physical” or “physico-chemical” concepts, since the superresolution image is a direct consequence of the molecular transition employed. Another hallmark is that they define, by the position of the intensity zero of the light used, where the molecules are “on” and where they are “off,” in other words, where the bright and where the dark states are established. They operate with any number of molecules, from single to many.

The concept of switching is also essential in more recent *far*-field fluorescence nanoscopy approaches [43–45], which differ from the previous ones by the fact that they switch molecules stochastically in space and utilize mathematics to assemble the image. Also very powerful, these concepts complement the earlier approaches. Therefore, after a brief excursion to an important all-optical improvement of the microscope’s axial resolution, I will review the field of *far*-field optical nanoscopy with emphasis on the breaking of the diffraction barrier. In particular, I will show that all fluorescence nanoscopy concepts realized so far utilize a transition between two distinguishable states of a marker, a bright and a dark state, to record fluorescent objects at sub- $\lambda/2$ distances sequentially in time. The transition between these states is operated as a fluorescence switch. Additionally, I will classify these concepts according to the states used and show that they differ on whether the switching and sequential recording occurs at predefined sample coordinates (and thus inherently on molecular ensembles) or stochastically in space, molecule by molecule.

19.2 Improving the Axial Resolution by Combining the Aperture of Two Lenses

The z -resolution of any standard *far*-field light microscope is at least three times poorer than that in the focal plane which is particularly limited in 3D-imaging transparent objects such as cells. Therefore, in the quest for nanoscale resolution in *far*-field optical microscopy, it was most natural to start out with the axial resolution problem.

The reason for the poorer axial resolution is that the focal diffraction spot is elongated along the optic axis ($\Delta z > \Delta r$). This elongation stems from

the fact that the focal spot is formed by the self-interference of a spherical wave front cap [3]. If the wavefront were a sphere instead of a cap, it would yield a spot that would be nearly spherical and hence a z -resolution that would be similar to its lateral counterpart. In other words, the lack of symmetry in focusing with respect to the focal point leads to a poorer z -confinement of the diffraction maximum. The same consideration holds for collecting the nearly spherical wavefront of fluorescence emitted from the dye [32, 46]. Expanding the wavefront for illumination or fluorescence collection is equivalent to expanding the microscope's aperture. It is the key physical element in spot-scanning 4Pi microscopy [32, 33, 46] and also in the widefield I⁵M [47].

4Pi microscopy improves the total aperture of a far-field fluorescence microscope through coherently adding the light fields of the spherical wavefront caps of two large-angle lenses for excitation or detection, or for both (Fig. 19.1b) [32, 46]. The two wavefront caps of excitation light interfere constructively at the common focal point, whereas the two emerging fluorescence wavefront caps interfere constructively at a common point of detection. Had each of the lenses a semi-aperture angle, $\alpha = 90^\circ$, the central focal diffraction spot would approach a spherical shape with a diameter of $\sim \lambda/3n$. Unfortunately, the available lenses feature only $\alpha \approx 68^\circ < 90^\circ$ which means that part of the nearly spherical wavefront is missing. The axially sharpened main diffraction spot of $\Delta z \approx \lambda/3n$ is accompanied by smaller yet pronounced side-lobes above and below the focal plane [46, 48], making the axial separation of objects ambiguous. Removing the (effect of the) lobes and making the 3D imaging unambiguous was the actual scientific challenge in this quest [49].

The first solution to this problem was to excite the fluorophore by two-photon absorption [33], because, among other effects, the quadratic dependence of the fluorescence on the excitation intensity rendered the contributions from the lobes so small that they could be unambiguously removed in the data by mathematical deconvolution [50]. As a result, two-photon excitation 4Pi microscopy provided images with substantially improved axial resolution in far-field fluorescence imaging [48, 51]. Microtubules or actin fibers, that were mingled in a confocal xz -image of a cell ($\Delta z \approx 500\text{--}600$ nm) could be clearly separated by 4Pi recording ($\Delta z \approx 140$ nm) [51–53]. Further developments, including that of multiple spot scanning and of a compact commercial instrument, provided a range of $\Delta z = 70\text{--}150$ nm in the 3D-imaging both in fixed and living cells [54–56]. 4Pi instruments have provided axially superresolved 3D images of H2AX chromatin clusters in the nucleus [57] in fixed cells, as well as of the mitochondrial 3D network and the Golgi apparatus in living cells [54, 58].

Novel field-corrected lenses of $\alpha = 74^\circ$ have recently enabled dual-color 4Pi recordings also with regular one-photon excitation [59, 60]. Still applying two-photon excitation with such lenses yielded a solitary central spot of $\Delta z \sim \lambda/3n$ with negligible lobes [61] (Fig. 19.1b). The creation of such a nearly spherical

solitary focal spot in 3D just by physics and its application to imaging has been a longstanding goal in the quest for far-field axial superresolution.

To provide widefield imaging, I⁵M [47, 62, 63] illuminates with plane (unfocused) interfering waves, rather than focused spherical wavefronts. Plane waves yield a standing wave pattern with many equidistant ($\lambda/2n$) layers of equal brightness along the z -axis. These multiple peaks render z -separation ambiguous, unless for the trivial case that the object is thinner than $< \lambda/2n$. This is why the so-called standing wave microscope (SWM) [64] strictly fails to provide axial superresolution for an arbitrary object in 3D [49, 58, 65, 66]. In the spatial frequency domain, the ambiguity is explained by the missing frequency bands inside the optical transfer function (OTF). I⁵M alleviates this problem by collecting the fluorescence like a 4Pi microscope, i.e., by coherently adding the spherical wavefronts caps of fluorescence light at a common detection point [49]. Compared to 4Pi microscopy, I⁵M trades off focused 4Pi-like illumination for widefield imaging capability. While it thus is more prone to ambiguities [67], I⁵M, unlike SWM, clearly is a self-consistent concept for axial resolution improvement.

The practical z -resolution increase from 400–800 nm down to 70–150 nm, i.e., by 3–7-fold, constituted the first substantial resolution improvement in far-field optical microscopy in many decades [48, 51–53, 63]. As a result, 4Pi and I⁵M imaging most visibly challenged the notion of the time that far-field resolution was a closed matter and near-field optics the only way to go.

On the same note, 4Pi microscopy features the largest aperture and hence the smallest focal spot. Yet it does not break the diffraction barrier; it just pushes diffraction to its limits.

19.3 Breaking the Diffraction Barrier

Let us assume an unknown number of tiny fluorescent objects or molecules that are $D < 200$ nm apart. If they all have different colors, one can separate them with the right excitation or emission filters. Discerning objects or molecules having distinct spectral characteristics is not really challenged by diffraction. The problem was to discern an *arbitrary* number of “identical” features at *arbitrary* distances $< \lambda/(2n \sin \alpha)$.

So, which phenomenon provides a solution for separating “identical” (fluorescent) objects closer than $\lambda/(2n \sin \alpha)$? The answer is switching the fluorescence (or more generally the signaling) capability of these adjacent objects on and off so that they can be registered separately. This is exactly how scanning STED microscopy resolves objects that are closer than the diffraction limit, whereby the switching of the fluorescence capability of the molecules is accomplished with a (STED) beam [35]. As a matter of fact, fluorescence switching or modulation is used in all far-field fluorescence microscopy concepts with “diffraction-unlimited” resolution currently employed (Fig. 19.2).

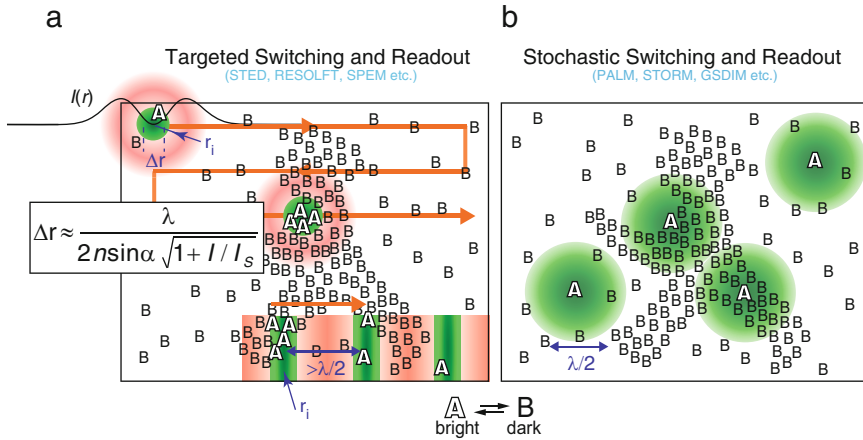


Fig. 19.2. All far-field fluorescence nanoscopy concepts realized so far switch the fluorophore between two distinguishable states, a bright state A and a dark state B , to construct subdiffraction images. The sketched object consists of molecules initially residing in B . The task of the superresolving concept is to bring features or molecules that are closer than the diffraction limit sequentially in the bright state A . This task can be accomplished either by establishing A at specific (targeted) spatial coordinates, or by letting the state A emerge stochastically. In both cases, the neighboring molecules have to be kept dark (in B). (a) Targeted readout mode: state A is established in a subdiffraction-sized spot of diameter Δr that is centered around the coordinate r_i . Featuring a zero at r_i , the role of the intensity distribution $I(r)$ (sketched in red) is to ensure that the molecules remain in B (when eliciting the transition $B \rightarrow A$). All the fluorophores from the spot with diameter Δr are read out simultaneously. The number of read-out (state A) fluorophores is determined by Δr and the local concentration of the molecules at the coordinate which is targeted by the spot. The image is assembled by translating the zero in space. As the zero is translated across the object, the molecules undergo several times the transition $B \rightarrow A \rightarrow B$, which is why this concept requires a reversible transition $A \leftrightarrow B$. The zero can also be line-shaped or an array of zero-lines, preferably of distance $> \lambda/(2n)$. (b) The stochastic readout mode detects single fluorophores from a random position within the diffraction zone. To this end, a molecule is transferred to a state A which is able to emit $m \gg 1$ photons in a row. The neighboring molecules remain in the dark, owing to an inherent inhibition preventing $B \rightarrow A$. The closest molecule in state A should be further away than the diffraction limit $\lambda/(2n)$. The detection of $m \gg 1$ photons allows the calculation of the coordinate of emission from the centroid of the diffraction fluorescence spot formed on a camera. After the recording, the molecule is switched off to B in order to allow the recording of an adjacent molecule. If it is sufficient to record a single picture, the stochastic read-out requires each molecule to cycle only once $B \rightarrow A \rightarrow B$. Both strategies assemble an image by registering fluorophores or fluorophore ensembles sequentially in time and both concepts utilize a mechanism that keeps the neighboring molecules dark (in state B). States A and B can also be reverted

To switch fluorescence, it takes two states: a bright (fluorescent) state A and a dark state B that are connected by a transition which is the actual switch. Several states in a fluorophore are suitable for such transitions (Fig. 19.3). The fluorescent singlet state S_1 and the ground state S_0 used in STED microscopy is the most basic and obvious pair of bright and dark states [39], but other examples will be given later, when discussing various nanoscopy implementations.

Fluorescence switching can be employed in two ways [68]. In the first option, the switching is carried out in a spatio-temporally controlled way, that is, one defines the coordinates where the states (A or B) are created in the sample using a dedicated spatial distribution of light. As one knows where the signal comes from, assembling an image becomes straightforward. This strategy is conceptually the most general one because it yields subdiffraction resolution images just by inducing molecular transitions (between a signaling and a non-signaling state). It is general, because no specific conditions are required for the way the state A has to signal. It is called the *targeted switching and read-out mode* [68]. The second option here called *stochastic switching and read out* [68] is to switch on and off individual molecules stochastically in space. This strategy is viable under the condition that the state A is able to emit $m \gg 1$ photons so that these photons can be associated with the same molecule, e.g. in a burst. In this case, the coordinate of molecular emission has to be found out (mathematically) after registering the photons with a camera. The two switching and read-out options are sketched in Fig. 19.2 and will be discussed in Sect. 19.3.1.

19.3.1 Targeted Switching and Read-out Mode: STED, GSD, SPEM/SSIM, RESOLFT

In the targeted read-out mode, the bright state A is established at coordinate r_i by driving an optical transition $A \rightarrow B$ with a light intensity distribution $I = I(r)$ featuring an intensity minimum, ideally a zero, at coordinate r_i (Figs. 19.1d and 19.2a). Applying $I(r)$ transfers the markers virtually everywhere to B , except at the zero-intensity point r_i where the molecules can still remain in A . The rate of the transition $A \rightarrow B$ is given by $k_{AB} = \sigma I$, with σ denoting the optical cross-section for $A \rightarrow B$. In order to effectively switch the molecule to B , the optically induced rate k_{AB} must outperform any competing spontaneous transitions between A and B . Since these spontaneous rates are given by the inverse lifetimes $\tau_{A,B}$ of the states A and B , we obtain: $k_{AB} = \sigma I \gg (\tau_{A,B})^{-1}$. Therefore, applying an intensity I that is much larger than the “saturation intensity” $I_s = (\sigma \tau_{A,B})^{-1}$ shifts the molecule everywhere to B except in the proximity of the zero-intensity point r_i of $I(r)$. Thus, we obtain a narrowly confined region $r_i \pm \Delta r/2$ in which the molecule can still be in A . The width Δr of this region or spot is readily calculated as

$$\Delta r \approx \frac{\lambda}{2n \sin \alpha \sqrt{1 + aI_{\max}/I_s}}. \quad (19.1)$$

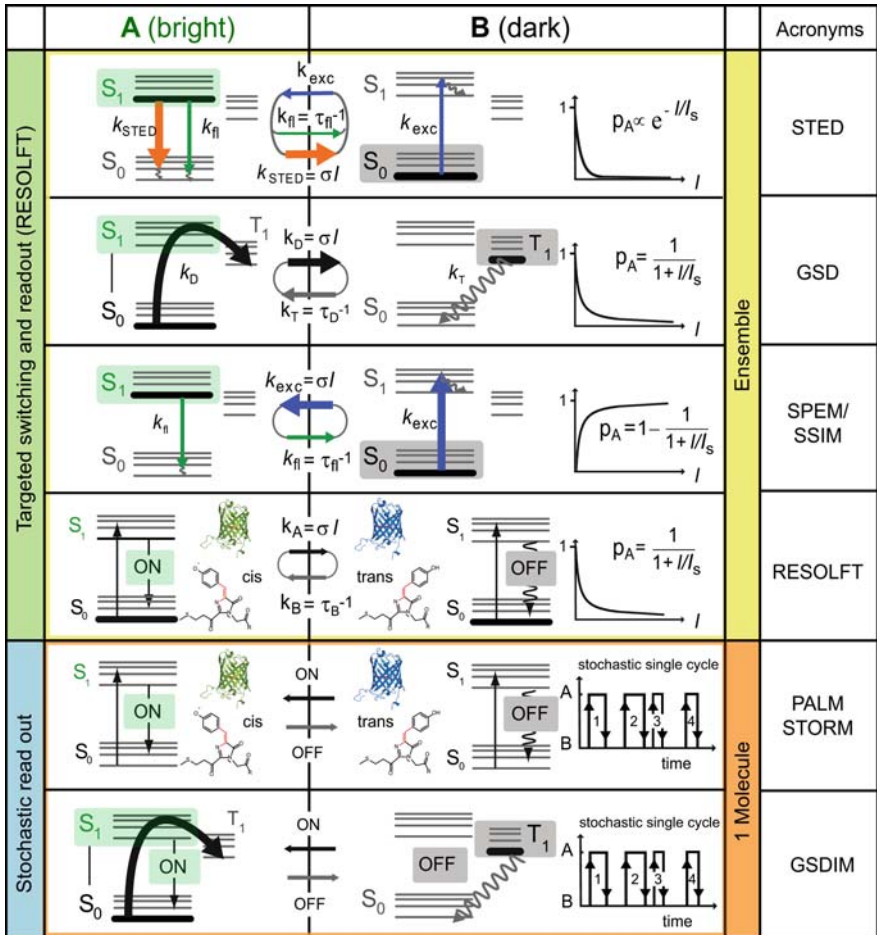


Fig. 19.3. Molecular transitions and states utilized to break the diffraction barrier. Each nanoscopy modality resorts to a specific pair of bright and dark states. Several concepts share the same states, but differ by the direction in which the molecule is driven optically (say $A \rightarrow B$ or $B \rightarrow A$) or by whether the transition is performed in a targeted way or stochastically. The targeted read-out modality drives the transition with an optical intensity I and hence operates with probabilities of the molecule of being in A or B . This probability depends on the rates k of the transitions between the two states and hence also on the applied intensity I . The probability p_A of the molecule to remain in A typically decreases as indicated in the panel. $p_A \ll 1$ means that the molecule is bound or “switched” to the state B . This switching from A to B or vice versa allows the confinement of A to subdiffraction-sized coordinates of extent Δr at a position r_i where $I(r)$ is zero. In the stochastic read-out mode, the probability that state A emerges in space is evenly distributed across the sample and kept so low that the molecules in state A are further apart from each other than the diffraction limit. An optically nonlinear aspect of the stochastic concept is the fact that the molecules undergo a switch to A from where they suddenly emit $m \gg 1$ detectable photons in a row

I_{\max} denotes the intensity of the peak enclosing the zero [39,41,69,70], whereas the optional prefactor a considers its shape [70]. For $I_{\max}/I_s \gg 1$, the spot Δr becomes much smaller than the diffraction limit.

A subdiffraction image with resolution Δr can now be readily assembled by scanning the zero-intensity point r_i across the object (Figs. 19.1d and 19.2a). In the process, the beam switches all molecules to the dark state B except those lying in the coordinate range $r_i \pm \Delta r/2$. As a result, the signal must originate from this range. Fluorophores closer together than Δr can be in the bright state A at the same time and hence can emit simultaneously. They cannot be resolved. However, fluorophores that are further away than Δr cannot be simultaneously in A ; they are registered sequentially in time and can be separated in the image. More generally formulated, narrowly spaced features or molecules are resolved in this scheme because features further away than the subdiffraction distance Δr are forced to reside in different states A and B . The prototype of this scheme is STED microscopy, where one feature can be in $A = S_1$ and its neighbor is forced by the STED beam to reside in $B = S_0$.

The subdiffraction resolution is given by Δr as defined in (19.1) [39, 41]. Since it is a far-field approach, the resolution still scales with λ , however, it is no longer *limited* by λ , because $I_{\max}/I_s \rightarrow \infty$ leads to $\Delta r \rightarrow 0$ [39, 41, 69]. The reason for the square-root law is that, in first approximation, the intensity $I(r)$ increases quadratically when departing from the zero-intensity point r_i .

Since diffraction precludes only the separation of objects lying closer than $\lambda/(2n \sin \alpha)$, the imaging process can be parallelized by implementing many zeros with distance $> \lambda/(2n \sin \alpha)$ from each other. In this case, the fluorescence can also be conveniently imaged on a camera (Fig. 19.1d). The whole scheme can be inverted [68] by exchanging A with B . Thus, it is also possible to confine the dark state B rather than the bright state A by applying a transition $B \rightarrow A$ (Fig. 19.1d).

Sequential readout at targeted coordinates in space is not only a hallmark of STED [35] but also of GSD microscopy [36], and other concepts exploiting reversible saturable or photoswitchable transitions $A \leftrightarrow B$ [42], including those that utilize many zeros in parallel such as saturated pattern excitation microscopy (SPEM) [71], which is also called saturated structured illumination microscopy (SSIM) [72]. They have been generalized under the acronym RESOLFT [39, 40] which is in fact synonymous with the targeted read-out mode. The resolution of all these concepts is governed by equation (19.1). Their OTF features an “infinitely expanded” frequency passband with an FWHM that scales with $1/\Delta r$ and hence with $\sqrt{I_{\max}/I_s}$ [73]. Again, the reason for the square-root law in the expansion of the passband is the quadratic rise of the intensity in the proximity of local intensity zeros.

As already indicated, in the targeted read-out mode, the fluorophores located within distance Δr remain indiscernible because they are in the same state (A or B) at the same time. If it is the bright state A (as in STED microscopy) this is clearly an advantage, because all the fluorophores located

within Δr add their signals. So, while the targeted read-out mode can certainly operate with and resolve single molecules, as such it is an ensemble concept dealing with any number of molecules. The number of molecules does not matter since the resolution is physically predefined by Δr which can be tuned through I_{\max}/I_s following (19.1). By the same token, the tuning of Δr allows one to adjust the average number of simultaneously recorded fluorophores which is very useful in many applications [74].

The power of this concept is underscored by the fact that several molecular states are able to take the role of A and B : basic electronic states, such as the S_0 , S_1 , the first triplet state T_1 , or “chemical” states, such as conformational or binding states of the fluorophore [39,41] (Fig. 19.3). Since the resolution and performance of a practical microscope is strongly determined by the actual choice of states A and B , we will discuss the various approaches on the basis of the states employed.

19.3.2 STED Microscopy

STED microscopy uses the most elementary states possible: the S_1 as A and the S_0 as B (Figs. 19.1 and 19.3). Most STED microscopy implementations have so far utilized a focused excitation beam and a red-shifted, doughnut-shaped “STED beam” for de-exciting potentially excited fluorophores back to the ground state $S_1 \rightarrow S_0$ by stimulated emission (note that the many photons of the stimulating beam and the handful stimulated photons are discarded in the process) [35, 75–78]. The only role of the STED beam is to switch off the ability of the dye to fluoresce by confining it to the S_0 . Even if these molecules encounter an excitation photon, they will not fluoresce, because the STED beam keeps them “off.” This fluorescence off-switching is, of course, absent within the range Δr around the doughnut zero.

To switch off the dye by STED, the stimulated emission rate $A \rightarrow B$ has to outperform the spontaneous decay rate of the S_1 which is given by its inverse lifetime $\tau_{\text{fl}} \approx 10^{-9}$ s. With $\sigma \approx 10^{-16}$ cm², $I_s = (\sigma\tau_{\text{fl}})^{-1}$ typically amounts to 3×10^{25} photons cm⁻² s⁻¹, i.e. ~ 3 –10 MW cm⁻². If exposed to the STED beam, the probability of a molecule to reside in S_1 decreases in first approximation as $\exp(-I/I_s)$. To confine S_1 in space, the STED beam is prepared to feature a zero; usually it forms a doughnut with crest intensity I_{\max} . Following (19.1), $I_{\max} \gg I_s$ confines the area in which the fluorophore can reside in S_1 to subdiffraction dimensions Δr around the doughnut zero. Scanning the zero across the sample registers features with subdiffraction resolution Δr sequentially in time.

Because $I_s = 3$ –10 MW cm⁻², STED microscopy operates with focal intensities $I = 0.1$ –1 GW cm⁻². While these intensities are 10–100 times larger than the typical intensities used for excitation, regarding photodamage or excitation by the STED beam one has to keep in mind that the wavelength of the STED beam is adjusted to the red edge of the emission spectrum of the dye, that is to a range where the molecule has a $> 10^4$ times reduced

excitation cross-section. Besides, the intensities required for STED are by 20–1,000 times lower than the 200 GW cm^{-2} required for live-cell compatible multiphoton microscopy in (sub)picosecond pulses [20, 79]. The reason is that stimulated emission requires just a single photon. The need for elevated intensities just stems from the requirement that $I \gg I_s$, that is the state S_1 has to be deactivated within its nanosecond lifetime τ_{fl} . Therefore, STED microscopy can be effectively implemented both with pulsed and with continuous wave (CW) lasers [80].

The local minimum, i.e. the ‘zero’, need not be formed as a doughnut; it could also be a groove [69, 78, 81] in which case the resolution would be improved just in the direction perpendicular to the groove. In fact, early demonstrations utilized just a laterally offset STED beam [76, 82], because of technical simplicity. Making special “doughnuts” having a strong peak above and beneath the focal plane (Fig. 19.1c), rendered $\Delta z = 100 \text{ nm}$ with a single lens [77], but the narrower STED zeros obtained from using 4Pi systems made $\Delta z = 33\text{--}60 \text{ nm}$ possible [83, 84]. Displaying an ~ 15 -fold improved axial resolution over confocal microscopy in the imaging of microtubules in fixed mammalian cells [84], these early STED-4Pi combinations demonstrated the potential of a far-field fluorescence microscope to operate in the tens of nanometers range [39].

Experiments using single molecules as test objects displayed a resolving power of 28–40 nm [81] and later $\Delta x = 16 \text{ nm}$ in the focal plane [69]. These experiments confirmed equation (19.1) and showed that a focal plane resolution of $\sim \lambda/45$ was achievable [69]. Applying this resolution in immunofluorescence imaging has initially been hampered by photobleaching, but allowing long-lived fluorophore dark states to relax, enabled $\Delta r = 20\text{--}30 \text{ nm}$ also in cells [85, 86]. A recent STED-4Pi combination called isoSTED demonstrated a nearly spherical, isotropic 3D-resolution of 40–45 nm [87]. Setting the current benchmark, such novel combinations of STED and 4Pi microscopy are likely to push all-molecular-physics-based isotropic resolution to values $< 15 \text{ nm}$.

Although STED and confocal microscopy are easily combined to each others advantage in the same setup, STED is not an extension of confocal microscopy, because it does not require the imaging of the fluorescence onto a pinhole. In principle, one could detect the fluorescence signal right at the sample. Therefore, parallelized camera-based STED microscopy will also be possible with arrays of doughnuts or lines (Fig. 19.1d) [88].

STED microscopy has been applied to study the fate of synaptic vesicle proteins during exocytosis. The study revealed that, when the vesicles fuse with the presynaptic membrane, the protein synaptotagmin *I* forms integral nanosized clusters at the synapse [89]. Since the clusters are similar in size and molecular density as integral vesicles, the study indicated, that entire protein clusters are taken up from the neuronal membrane when forming new vesicles. By the same token, this initial application of far-field fluorescence nanoscopy

to a biological problem demonstrated the potential of this emerging field for solving longstanding problems in the life sciences.

In another application, STED microscopy also revealed the ring-like structure of the protein *bruchpilot* at synaptic active zones in the drosophila neuromuscular junction [90]. Further studies included the visualization of the spatial distribution of the SNARE protein syntaxin [91], the nuclear protein SC35 [85], and the nicotinic acetylcholine receptor [92]. IsoSTED microscopy resolved the tube-like 3D-distribution of the TOM20 protein complex in the mitochondria in a mammalian cell [87].

The viability of STED microscopy with living cells was demonstrated in its early stages [77]. However, focusing on optical aspects of the concept, those experiments were carried out with slow piezo-scanning stages. Recent fast galvanometer-scanning implementations of STED microscopy [93] visualized the rapid motion of dense synaptic vesicles at the synapse of living hippocampal neurons at video rate [94]. These results showed that nanoscale resolution and the visualization of rapid physiological processes can be reconciled, on the basis of existing physical principles and with available technology.

The nanosized detection area Δr or volume created by STED also extends the power of fluorescence correlation spectroscopy (FCS) and the detection of molecular diffusion [74, 95]. For example, STED microscopy has probed the diffusion and interaction of single lipid molecules on the nanoscale in the membrane of a living cell (Fig. 19.6). The up to ~ 70 times smaller detection areas created by STED (as compared to confocal microscopy) revealed marked differences between the diffusion of sphingo- and phospholipids [74]. While phospholipids exhibited a comparatively free diffusion, sphingolipids showed a transient (~ 10 ms) cholesterol-mediated “trapping” taking place in a < 20 -nm diameter area, which disappeared after cholesterol depletion. Hence, in an unperturbed cell putative cholesterol-mediated lipid membrane rafts should be similarly short-lived and smaller.

Stimulated emission occurs in all dyes investigated. Yet, just as in experiments using single molecules, the utility of a number of dyes will be precluded by bleaching. Nonetheless, several suitable organic dyes were found in each part of the spectrum. In any case, the general demand for increased photostability is leading to the design of new labels with increased potential for STED microscopy, including fluorescent proteins. STED on yellow fluorescent proteins [96] has recently been used in an application that quantified morphological changes in dendritic spines in living organotypical hippocampal brain slices upon external stimulation [97].

STED microscopy has important applications outside biology as well. For example, it currently is the only method to locally and noninvasively resolve the 3D assembly of packed nanosized colloidal particles [98, 99]. In the realm of solid-state physics, STED microscopy has recently imaged densely packed fluorescent color centers in crystals, specifically charged nitrogen vacancy (NV) centers in diamonds [100]. NV centers in diamond have attracted attention, because of their potential application in quantum cryptography and

computation, but also for nanoscale magnetic imaging [101, 102]. Since NV centers do not bleach or blink upon excitation, nanoparticles of diamond containing NV centers are also being developed as nonbleaching labels for bioimaging [103, 104].

Figure 19.4 shows that these centers enable a virtually ideal implementation of the STED concept. The population of the bright state decreases with the intensity I , as one would expect from theory: $\exp(-I/I_s)$. If $I \gg I_s$, the linear representation of the exponential fluorescence “depletion curve” appears to be “rectangular” [35], meaning that one can have a very narrow intensity range $I < I_s$ in which the NV centers are “on” and a broad intensity range $I \gg I_s$ where the center is “off.” As a result, STED microscopy was capable of imaging NV centers with a resolution of $\Delta r = 16\text{--}18$ nm in raw data. Once separated by STED, the position of the NV centers can then be calculated with Ångström precision. Recording could be continually repeated without degradation of resolution or signal, proving far-field nanoscale imaging without photobleaching. At the same time, these results underscore the potential of NV containing diamond nanoparticles for biolabeling. Last but not the least, increasing I yielded $\Delta r = 5.8$ nm, demonstrating an “all-physics-based” resolving power exceeding the wavelength of light by 2 orders of magnitude [100]. These experiments corroborate the prediction of the original paper [35] that “rectangular depletion curves” would allow increasing the far-field resolution to “infinity.”

19.3.3 Ground State Depletion (GSD) Microscopy

GSD microscopy [36, 75] was the second concretely laid out concept to overcome the diffraction barrier. Although related to STED microscopy, it uses an entirely different mechanism for switching off fluorescence. To allow for much lower intensities, the fluorophore is switched off by transiently shelving it in the metastable triplet state T_1 serving as the dark state B . The bright state A is now the S_0 , or more precisely, the dye’s singlet system (Fig. 19.3). The transfer to the T_1 is accomplished by repeated $S_0 \rightarrow S_1$ excitation, so that the dye is eventually “caught” in the T_1 . Reading out the fluorescence of A is performed at the same wavelength. Due to the fact that the T_1 lifetime of $\tau_T = 1\ \mu\text{s} - 1\ \text{ms}$ is now by 3–6 orders of magnitude longer than τ_F , I_s is reduced by the same factor. Using this mechanism, the dye can be switched off at $10^3\text{--}10^6$ times lower intensities than with STED, still giving similar resolution [36, 75].

GSD microscopy has been shown to image immunolabeled protein clusters on the plasma membrane of fixed cells with $\Delta r = 50\text{--}90$ nm resolution using a CW laser power of a few kilowatt per square centimeter [105]. However, plain GSD microscopy is currently challenged by the fact that the repeated population of the triplet state or similar dark states augments photobleaching [105]. Nonetheless, this early concept was important for the development of far-field optical nanoscopy for a number of reasons. First, it highlighted

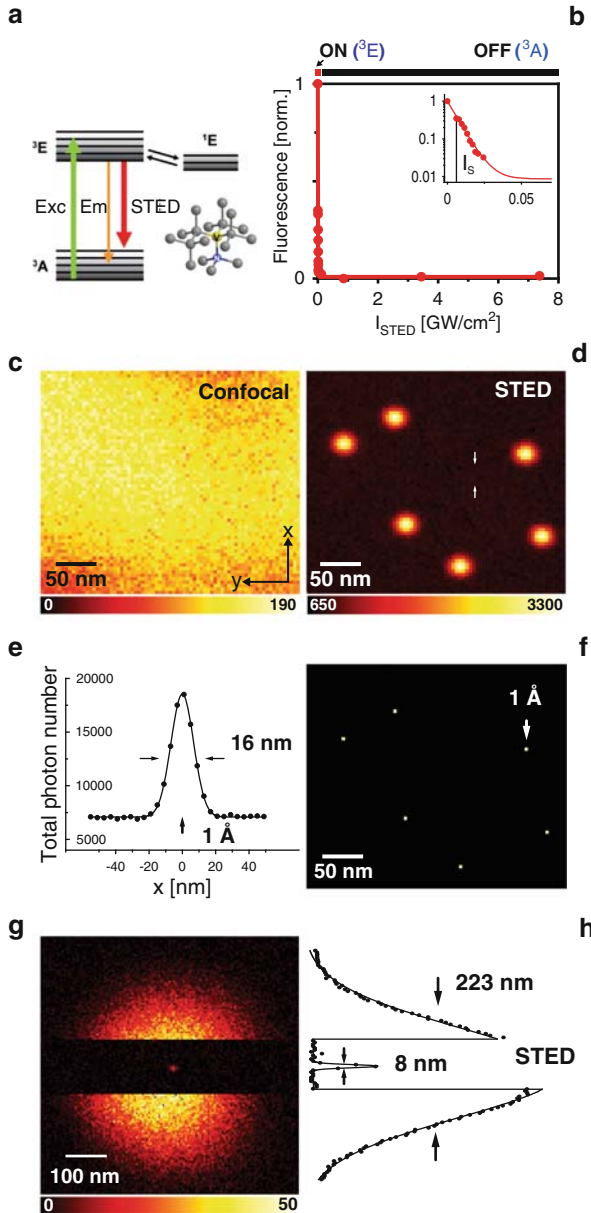


Fig. 19.4. Stimulated emission depletion (STED) microscopy reveals densely packed charged nitrogen vacancy (NV) color centers in a diamond crystal. (a) State diagram of NV centers in diamond (see inserted sketch) showing the triplet ground (3A) and fluorescent state (3E) along with a dark singlet state (1E) and the transitions of excitation (Exc), emission (Em), and stimulated emission (STED). (b) The step decline in fluorescence with increasing intensity I_{STED} shows that the STED-beam is able to “switch off” the centers almost in a digital-like fashion. This nearly “rectangular”

that other processes but stimulated emission – in fact, “any transition in a fluorophore that nondestructively inhibits fluorescence” [75] (i.e. keeps the molecule dark) – could be used to overcome the limiting role of diffraction. Second, whereas switching off the fluorescence capability of the dye by STED requires the presence of light, the GSD concept is the first to use a “genuine” molecular switch: flipping an electron spin switches the dye to a relatively long-lived dark state in which it is deactivated. Back-flipping, i.e., the return to its singlet states, means that the dye is switched on again. Thus, within a period τ_T , GSD provides optical bistability.

19.3.4 Saturated Pattern Excitation or Saturated Structured Illumination Microscopy

SPEM/SSIM [71, 72] differs from GSD or STED in that it confines the dark state B rather than the bright state A (Fig. 19.1d), thus producing “dark” regions in which the dye remains in B (S_0) that are steeply surrounded by areas in which it is switched to A (i.e., S_1) [39, 68]. Applying $I_{\max} > I_s$ confines these dark regions to subdiffraction dimensions Δr following (19.1). Since it produces “negative data,” the images have to be reconstructed computationally. Recording is also performed by scanning an array of line-shaped zeroes in the direction orthogonal to the lines and reading out the data with a camera for each scanning step. In order to cover all directions, the array is rotated an adequate number of times [72]. I_s is similar in magnitude as in the STED concept, because it relies on the same states. SPEM/SSIM

Fig. 19.4 (Continued). excited state depletion curve testifies a close to ideal implementation of the STED effect. The half-logarithmic inset representation of the depletion curve confirms the exponential optical suppression of the excited state. For $I_{\text{STED}} > 20 \text{ MW cm}^{-2}$, the center is in essence deprived of its ability to fluoresce, i.e., switched off. The “on-off” optical switching facilitates far-field optical separation of NV centers on the nanoscale. While the confocal image (c) from the very same crystal region is blurred and featureless, the STED image (d) reveals individual NV centers. The notion that these are single color centers is supported by the fact that they are similar in brightness and appearance. The spot produced by the individual centers represents the effective point-spread-function (PSF) of the STED recording. An exemplary y -profile of the PSF is shown in (e), revealing a lateral resolution $\Delta y = 16.1 \text{ nm}$. Once the NV centers are resolved, and provided that scanning errors can be neglected, the location of each center can be calculated with Ångström precision, as exemplified in panel (f) which should then be contrasted with panel (c). Panel (g) shows data from a similar experiment, demonstrating a 777-fold sharpening of the effective focal spot area through STED. As depicted by the profile in (h) the spot diameter is decreased from 223 nm down to 8 nm. Note that the increase in resolving power is a purely physical effect, i.e., just based on state transitions. The steep optical off-switching of the NV centers depicted in panel b indicates that optimizing the process is bound to improve the far-field optical resolution further

displayed a lateral resolution of 50 nm with beads (obtained after the mandatory computation) [72]. SPEM/SSIM can also be explained in the spatial frequency domain with the OTF [71, 72]. Like STED and GSD, the OTF of SPEM/SSIM is “unlimited,” featuring an FWHM scaling with $1/\Delta r$ and hence with $\sqrt{(I_{\max}/I_s)}$ [73].

19.3.5 Photoswitching in the Generalized RESOLFT Concept

The conception of GSD microscopy to reversibly switch the fluorophore to a metastable state has led to the consideration of molecular switches between states of even longer lifetimes. As a matter of fact, the ultimate saturable or switching transition occurs between two stable states [38–41]. The advantage of switching between two stable states is obvious: since there are no spontaneous interstate transitions, it follows that $I_s \rightarrow 0$. As a result, it should be possible to implement huge values I_{\max}/I_s which, following (19.1), should yield very small Δr even at low I_{\max} .

Switches between long-lasting molecular states can be realized through conformational changes such as photoinduced cis-trans isomerization between a fluorescent isomeric state A and a dark counterpart B . In other words, the reversible spin flip of the GSD concept is replaced by the relocation of an atom or a group of atoms in the molecule. Other options are bistable binding events, ring-opening, or closing reactions, etc. Concrete examples of reversible photoswitching are found in reversibly photoactivatable GFP-like proteins, such as *asFP595* [106] and *dronpa* [107], and in photochromic organic compounds. For this reason, it has been proposed to utilize photoswitchable proteins and fluorescent photochromic compounds to break the diffraction barrier in the targeted read-out mode [38, 39, 41, 108]; the concept was called RESOLFT [40].

The fluorescence is gained by exciting the dye from this (conformational) state A to an electronically excited, fluorescent state A^* and recording the emission $A^* \rightarrow A$, at the same time as the surrounding molecules are kept in the dark state B . Experiments with the reversibly photoactivatable *asFP595* indeed demonstrated for the first time the overcoming of the diffraction barrier by switching photoactivatable proteins [42]. As anticipated, this could be accomplished using intensities $I_{\max} \approx 10 \text{ W cm}^{-2}$, which are by 6 orders of magnitude lower than those required for STED. These results also verified the prediction [38–42] about the huge potential of switching photoactivatable proteins and photochromic (photoswitchable) organic dyes for overcoming far-field microscopy diffraction barrier.

Conversely, these experiments [42] also revealed the challenge currently encountered with switching fluorophores reversibly between A and B using a light intensity featuring a local zero: it is the finite number of switching cycles. Unfortunately, a fair number of cycles are required when defining the coordinates of the states A and B in the sample (Fig. 19.2). This stems from the fact that ensuring the exclusive presence of state A at a subdiffraction-sized

coordinate $r_i \pm \Delta r/2$ necessitates fluorophores outside this subdiffraction-sized region to stay in B . So, if these fluorophores happen to cross to A , they must be optically pushed back to B , in which case they have undergone a switching cycle without contributing signal. For this reason, in a targeted read-out modality (RESOLFT concept) the number of possible $A \leftrightarrow B$ cycles that a molecule can undergo before degradation has to be considered. In the simplest case, improving the resolution by a factor of m in the focal plane forces the fluorophore to undergo about m^2 switching cycles due to the m -fold finer targeting (scanning) steps. Likewise, m^3 cycles are required if the same improvement is implemented in 3D. Thus an improvement by a factor of 10 easily entails 100–1000 cycles.

19.3.6 Stochastic Switching and Read-out Mode: PALM, STORM, GSDIM

The challenge posed by repeated $A \leftrightarrow B$ cycling is alleviated when switching individual molecules stochastically in space. In this approach, molecules that are initially in the dark state B pop up individually in A at unknown coordinates r_i . A restriction on the bright state A is that it must be able to give off many photons in a row (e.g., through repeated excitation $A \leftrightarrow A^*$) so that it renders a diffraction blob of $m \gg 1$ detected photons when imaged onto a camera. (At least one must be able to associate m detected photons with the state A .) During this process, the surrounding molecules do not cross to A due to an inherent inhibition; they remain dark. The detection of $m \gg 1$ photons from the same bright molecule is a distinct requirement of the stochastic switching mode, because the molecular position r_i has to be obtained by calculating the centroid of the blob, which can be done with subdiffraction precision $\sim \lambda/(2n \sin \alpha \sqrt{m})$ [109, 110]. Called localization, this calculation rests on the assumption that the blobs on the camera represent single (or few identifiable) molecules, which is the case if the distance between two A state molecules is about $> \lambda/(2n \sin \alpha)$. After the coordinate of the A state molecule has been read out it is switched off again $A \rightarrow B$, to allow reading out a neighboring molecule using the same cycle $B \rightarrow A \rightarrow B$. The image is assembled molecule by molecule.

Whereas in the targeted read-out mode, a molecule has to undergo many cycles $A \leftrightarrow B$, in the stochastic switching mode, a single cycle $B \rightarrow A \rightarrow B$ per molecule is enough to produce an image [68]. Thus, this mode largely avoids switching fatigue. If the object needs to be imaged repeatedly, the same molecule has to be engaged repeatedly. In this case, several cycles per molecule are needed. Yet the number of cycles is still smaller than in the targeted read-out mode, because the molecules are switched only when they are supposed to contribute with a signal [68].

This strategy of combining stochastic molecular switching with localization has been used in the methods called SHRIMP [111] and NALMS [112], in which the position of a small number of bright regular fluorophores (in

state A) was mapped by bleaching them down stochastically to a final dark state B . However, as these methods started out from many A state (bright) molecules and hence from a bright total signal, they could accommodate only a small number of fluorophores. The strategy of combining stochastic switching and localization for an arbitrary number of molecules [43–45, 113, 114] has been realized in the methods called photoactivatable localization microscopy (PALM) [43] and stochastic optical reconstruction microscopy (STORM) [44] or fluorescence photoactivatable localization microscopy (FPALM) [45]. In these studies, photoswitchable proteins or photochromic compounds were optically driven from the dark state B to the bright state A by means of a photon absorption (i.e., optically activated), localized, and finally sent back to B . So, while SHRIMP and NALMS used only a half cycle out of a bright state $A \rightarrow B$, PALM and STORM now used a full cycle $B \rightarrow A \rightarrow B$. Starting out from the dark state B they could get rid of the bright initial signal of state A molecules and hence could accommodate an arbitrary number of them.

Importantly, some molecules may be localized more precisely than others, because the number of photon emissions m follows a statistical distribution. Therefore, to ensure a certain resolution, the stochastic read-out mode defines a brightness threshold (e.g., $m > M \approx 50$). Molecules with $m < M$ are discarded (bleached) without contributing to the image. In a sense the discarding of the molecules with $m < M$ is to the stochastic read-out what “switching fatigue” is to its targeted counterpart; the higher the required resolution, the more molecular events are discarded. M depends on the average number of photon emissions in the “on” state and the desired resolution, which, provided there is no background, exceeds $\lambda / \left(2n \sin \alpha \sqrt{M} \right)$. Clearly, just as the targeted read-out mode requires a large number of switching cycles for optimal performance, the stochastic mode requires a large M . Thus, at the expense of disregarding more molecules, PALM, STORM, and other variants of the stochastic read out have achieved a resolution of < 20 nm in the focal plane [43, 115–119].

PALM has first been accomplished by switching on activatable fluorescent proteins $B \rightarrow A$ using a dedicated beam of light, whereas the off-switching $A \rightarrow B'$ was accomplished through bleaching at the expense of being able to record only a single (or very few) images. Since B can be a different state than B' the requirements on the photoswitchable compounds are more relaxed [43]. In contrast, STORM was put forth with repeated cycling between the same dark states: $B = B'$ [44]. STORM imaging [115, 120] took advantage of the reversible cis-trans isomerization of organic cyanine molecules, in fact of (cyanine) molecule pairs, whereby one of them served as an activator molecule facilitating the switching of the other.

PALM and STORM inherently operate with ultra-low light levels for activating the fluorophore, because like the earlier RESOLFT experiments [42], they switch between the relatively long-lived (conformational) states of photoactivatable proteins or organic fluorophores, which entails very low I_s of $< 10 \text{ W cm}^{-2}$. Since activating more than about one molecule within a range $< \lambda / (2n \sin \alpha)$ has to be avoided, the intensity applied for switching

is further reduced by the number of molecules expected to reside within the diffraction range. In any case, the low intensity operation greatly simplifies the implementation of this concept in a widefield illumination arrangement [115, 121, 122].

PALM images of thin cryosections of lysosomal transmembrane protein in a mammalian cell displayed a resolution of < 30 nm [43]. The demonstration of PALM and STORM involved the time-sequential use of two chopped laser beams, one for switching on ($B \rightarrow A$) and the other one ($A \rightarrow A^*$) for producing the m photons and switching off ($A \rightarrow B$). The pulsed action of the lasers and the time-window of the camera read-out need to be synchronized in this case. This is different in the modalities “PALM with independently running acquisition” (PALMIRA) [118, 119] and ground state depletion followed by single molecule return (GSDIM) [123] in which no activation beam is used and the fluorophores are allowed to pop up ($B \rightarrow A$) stochastically in time (not only in space) after most of them have been pushed back to a dark state B [114, 123]. A single CW laser beam is used for generating the m photons through $A \rightarrow A^*$ and for switching the fluorophore off $A \rightarrow B$. The bursts of photons are detected by a fast freely operating camera, whereby the intensity of the laser is adjusted such that the average duration of the m -photon burst coincides within the duration of a camera frame ($\sim 1/500$ Hz = 2 ms). These purely stochastic concepts probably are the simplest far-field nanoscopy systems at present, because they require just uniform laser illumination, a freely running camera, and appropriate software. Even multiple color imaging [117, 123, 124] is possible using the same laser as exemplified in Fig. 19.5c.

GSDIM [123] stands out by the fact that, unlike PALM, STORM, or PALMIRA, this concept operates with fluorophores, such as rhodamines, that are considered ordinary and not “switchable.” Still, to provide nanoscale resolution, GSDIM has to employ a switching mechanism. As the name suggests, the switching mechanism is that of the old GSD concept [36]: Initially residing in the ground state S_0 (state A), the fluorophores are strongly excited with a spatially uniform CW beam so that, after a number of $S_0 \leftrightarrow S_1$ transitions, they are caught in the dark triplet state T_1 or similar metastable dark state B for a time τ_T of a few milliseconds. After τ_T , individual molecules stochastically return to the singlet system ($B \rightarrow A$) where they instantly give rise to a bunch of m photons, followed by a return to B . The advent of a concept [114] that switches the molecules to B and relies on their spontaneous return to A showed that the stochastic single molecule switching approach for nanoscopy is actually broader in scope than suggested by the first implementations. Moreover, the use of the very same switching mechanism both in a targeted (GSD) and in a stochastic way (GSDIM) underscores once more that, on a fundamental level, all the nanoscopy concepts discussed herein rest on common molecular ground.

An early description of the localization procedure is due to Heisenberg [109] who remarked that the emission of m photons from a resting emitter enables the calculation of its position with precision $\sim \lambda/(2n \sin \alpha \sqrt{m})$.

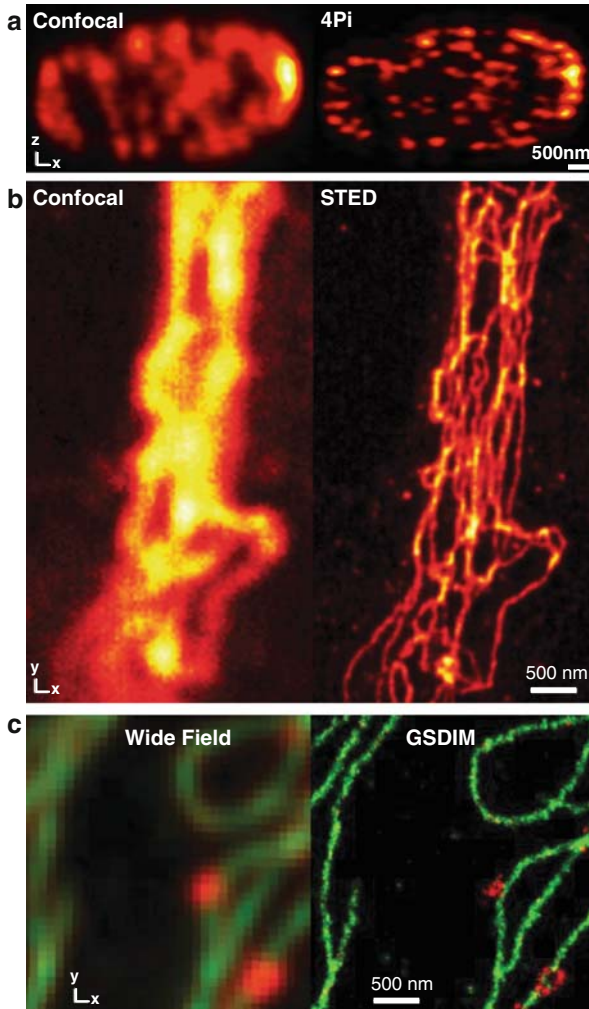


Fig. 19.5. Resolution increase exemplified in various techniques. (a) Confocal vs. 4Pi microscopy (xz -image) recorded from the microtubular network in a neuron, displaying an improved z -resolution of 140 nm. The 4Pi image data is due to an all-optically created narrow solitary peak, i.e., showing raw data. (b) Confocal vs. an STED image of immunolabeled vimentin in a mammalian neuroblastoma, after linear deconvolution, recorded using a compact supercontinuum STED-microscope with a spatial resolution < 25 nm. (c) Conventional widefield image compared with a GSDIM image of microtubules (*green*) and peroxysomes (*red*) in mammalian cells evidencing a substantial gain in image detail by far-field optical superresolution

However, finding out the position of an object with arbitrary precision is not the same as resolution, which is about separating similar objects at small distances. Localization per se cannot provide superresolution. This is also why, although it had been known and used for decades [109, 110] and even routinely applied to single molecules [125, 126], localization alone has not provided nanoscale images. (Note that in spite the use of localization in the 1980's and earlier, near-field optical microscopy still seemed to be the only way to attain nanoscale resolution up to the early 1990's.) Resolution clearly requires a criterion to discern objects or molecules, the simplest of which is "bright" vs. "dark."

In one particular study, it was shown that at low temperatures (1.2 K) the absorption spectra of individual pentacene molecules in a *p*-terphenyl crystal are so distinct (due to inhomogenous broadening) that one can address and localize (seven) fluorescent pentacene molecules individually at sub-diffraction distances by their absorption spectra. However, this interesting study left it unclear how superresolution by spectral separation could be extended to ambient conditions, to an arbitrary number of fluorophores (which is required to be a general imaging method), to other types of fluorophores, and thus become applicable [127].

In fact, assembling an image with the coordinates of fluorophores that are spectrally separated by cryogenic inhomogenous broadening had been suggested in an earlier theoretical study [128]. However, this study still proposed near-field optical microscopy as the best solution to the diffraction resolution problem. More importantly, this proposal fully relied on the *spectral* separation of molecules and did not suggest switching fluorescence on or off to record adjacent features sequentially, as is inherent in the earlier concept of STED microscopy [35] and in the GSD concept [36].

While extended molecular separation by spectral shifts is certainly interesting and may be eventually practical, the transition [111, 112] from single emitter localization to nanoscale imaging [43–45, 129] has thus not been facilitated by spectral separation, but by fluorescence switching. The reason why switching is so powerful for breaking the diffraction barrier is readily explained. Switching enables the separation of an arbitrary number of molecules or objects by stretching their signal out to an arbitrary number of time points, using just two distinguishable states A and B. Separation by color or wavelength requires a much larger – in principle arbitrarily large set of separable states (A, B, C, D, ..), which is hard to realize in an ordinary fluorophore. (In some special cases, an option could be to implement a state energy shift using an external field gradient as in magnetic resonance imaging.) Viable at room temperature and realizable with pairs of different kinds of bright and dark states, (fluorescence) switching is the essence of all nanoscopy concepts reported to date, irrespective of whether they operate with single molecules or ensembles. It is the element without which none of the nanoscopy concepts discussed herein could have produced an image.

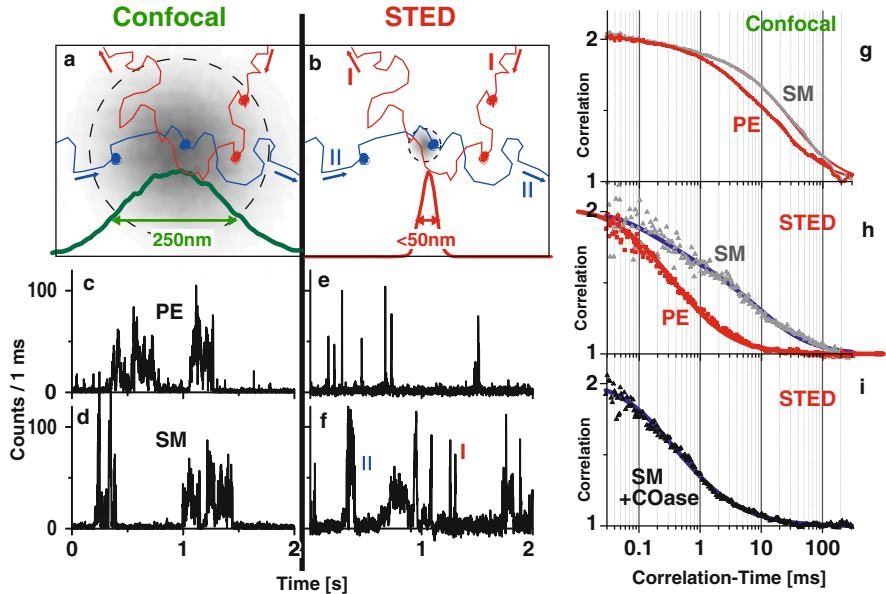


Fig. 19.6. STED microscopy discriminates the dynamics of single sphingo- and phospholipid molecules in a living cell membrane: dye-labeled sphingomyelin (SM) vs. phosphoethanolamine (PE). Panels (a) and (b) illustrate that freely moving molecules may be transiently trapped in the membrane due to interaction with another molecule. The passage time of freely diffusing molecules through the small spot created by STED is substantially reduced compared to that through a confocal microscope. c–f) Fluorescence bursts from labeled single PE and SM lipids detected with the 250-nm diameter confocal (c, d) and a 50-nm diameter STED spot (e, f) reveal that, by reducing the time that a freely diffusing molecule spends in the detection area, the smaller spot created by STED distinguishes free lipid diffusion (I) from interaction events (II) during passage through the spot. Panels (g)–(i) quantify the diffusion of PE and SM lipids on the plasma membrane using fluorescence correlation spectroscopy. Normalized correlation data of PE (*red dots*) and SM (*grey dots*) are compared for a standard confocal (g) and an STED recording (h) depicting the heterogeneous diffusion of SM. While in the confocal case the difference between the SM and PE diffusion could be explained just by a generally slower diffusion of SM, the STED recording can only be explained by a transient trapping just of SM. (i) Following depletion of cholesterol, the diffusion of SM (*black dots*) is similar to that of the rather freely diffusing PE. Thus, STED microscopy reveals cholesterol-assisted heterogeneous diffusion of SM on the nanoscale

19.4 Further General Aspects

The new pathway followed in STED and GSD microscopy was to spatially confine or isolate the bright molecular state by switching neighboring molecules off and keeping them dark. This change in strategy over earlier techniques is also reflected in the PSF of these microscopes. While earlier PSFs essentially

described focal intensity distributions in the microscope, the PSF of a STED or a GSD microscope mirrored the spatial distribution of fluorophore states – specifically of the fluorescent state as resulting from the molecular kinetics and the imposed optical dark state transitions.

When inducing an (incoherent) optical transition $A \rightarrow B$, the probability p_A of the molecule to be in state A is proportional to $\exp(-I/I_s)$ or, if there is an equilibrating rate $B \rightarrow A$, proportional to $(1 + I/I_s)^{-1}$ as sketched in Fig. 19.3 [39]. Due to the inherently nonlinear dependence of p_A on the intensity I , one can interpret STED, GSD, SPEM/SSIM, RESOLFT as nonlinear optical concepts. However, as it stems from the transition between two states, this nonlinearity is, of course, fundamentally different from m -photon absorption or scattering processes where the nonlinearity stems from the concomitant action of m photons. Moreover, these functions p_A bring about nonlinearities of infinite order $(\gamma I)^m$ with $m \rightarrow \infty$, which allow one to “break” the diffraction barrier by obtaining “infinite” optical bandwidth. By contrast, m -photon processes are firmly limited to order m , which in practice means $m < 3$. Since I_s can be decreased by selecting long-lived states, p_A enables huge nonlinearities even at low I [38–42].

By applying $I \ll I_s$, stochastic read-out modes such as PALM, STORM, and GSDIM clearly avoid a nonlinear dependence on the switching intensity. Still, nonlinear optical aspects are inherent to these concepts as well. They stem from the molecular switching and the burst of $> m$ photons originating from a single emitter, which has been shown to be connected with diffraction-unlimited far-field optical resolution [130]. Although a nonlinearity interpretation is applicable to all current nanoscopy concepts, it clearly is not specific enough to single out the facilitator which is the switching between two states $A \rightarrow B$.

All diffraction-unlimited nanoscopy methods can provide improved axial resolution even when implemented with a single lens [77, 83, 120, 131, 132]. However, because it starts out from less favorable values, the z -resolution usually remains worse than its focal plane counterpart. The coherent use of opposing lenses pioneered in 4Pi microscopy and I³M, however, facilitates an independent resolution improvement factor by 3–7-fold along the optic axis as has already been demonstrated with STED [83, 84, 87]. In the stochastic single molecule switching modalities, a similar gain in resolution will take place by the coherent use of opposing lenses [133]. Thus, while 4Pi microscopy and I³M did not break the diffraction barrier, they remain cornerstones of far-field fluorescence nanoscopy in the future.

Since 1994, it has been advocated that the key to nanoscale resolution is the imaged dye itself [34–36, 39, 41], making it worthwhile synthesizing fluorophores and other markers just for the purpose of overcoming the diffraction resolution limit [39, 41]. For the stochastic single molecule switching modalities, molecules are desired that burst out large m in the shortest possible period of time, while for the targeted switching the aim should be molecules that can be switched many times between a dark and a bright state.

Importantly, in the targeted read-out mode, the state A need not be fluorescent; in fact, not even an optical emitter, but just detectable through a specific signal [41]. This is because the coordinate is defined by the zero, and that is sufficient. In the stochastic switching mode, it is just the other way around. As it has been proposed [114] and shown [123], the state A need not be activated by light; the only requirement with regard to optics is that it emits m photons that can be detected on a camera. Since there are no fundamental reasons why markers will not improve as resolution facilitators, it is likely that the performance of all these concepts will improve substantially within the coming years. Therefore, emerging optical nanoscopy is bound to transform the life sciences and also impact other fields benefiting from noninvasive nanoscale (3D) optical resolution. In any case, the concepts and results reviewed herein already broke longstanding barriers of perception of what can be accomplished with a microscope that uses just focused visible light.

Finally, it is worthwhile imagining the possible ultimate resolution limits. So, if we had the perfect switchable marker emitting a bunch of $m \gg 10^6$ photons, what would we obtain for the stochastic single molecule switching mode? We would obtain the (average) position of a molecule with a precision of a fraction of a nanometer. While this information would be invaluable for mapping the sample, it would not tell us much about the molecule itself.

However, the situation is different in a purely transition based concept such as STED, in which the molecule is optically driven between two states at defined spatial coordinates. As a matter of fact, equation (19.1) is provocative because $I_{\max}/I_s \rightarrow \infty$ yields $\Delta r \rightarrow 0$. While this extreme extrapolation cannot be taken literally, it brings up the question as to what may happen if I_{\max} is indeed continually increased. Let us imagine a molecule of a nanometer in size, placed at the zero-intensity point of the electric light field driving the transition. If we now steadily increase I_{\max} , the light field becomes non-negligible at the periphery of the electron orbitals, while their central part would still be weakly exposed. Now, as different orbital parts experience fields of different strengths, these parts will have differently pronounced contributions to the optical transition. Hence, the extent of the molecule and its orbital can no longer be neglected with regard to the spatial structure of the light field. If we now translate the zero across the molecule, the probability of an optical transition $A \rightarrow B$, say excitation, stimulated emission, photoconversion, photo-isomerization, or whatever, will change as a function of the role of the excluded parts of the orbital in the transition. Translating the zero across the orbital should therefore yield information about the (dimensions of the) orbital and thus, about the molecule itself. No matter how quickly this “*inframolecular*” photophysics, photochemistry or exploration becomes reality, this fascinating prospect once more highlights the unexpected potential of investigating small scales in nature with freely propagating light.

References

1. E. Abbe, *Beiträge zur Theorie des Mikroskops und der mikroskopischen Wahrnehmung*. Arch. Mikr. Anat. 9, 413–468 (1873)
2. B. Alberts et al., *Molecular Biology of the Cell*. 4 edn. (Garland Science, New York, 2002)
3. M. Born, E. Wolf, *Principles of Optics*. 7th edn. (Cambridge University Press, Cambridge, New York, Melbourne, Madrid, Cape Town, 2002), p. 952
4. E.H. Synge, A suggested method for extending microscopic resolution into the ultra-microscopic region. *Philos. Mag.* 6, 356 (1928)
5. E.A. Ash, G. Nicholls, Super-resolution aperture scanning microscope. *Nature* 237 510–512 (1972)
6. D.W. Pohl, W. Denk, M. Lanz, Optical stethoscopy: Image recording with resolution $\lambda/20$. *Appl. Phys. Lett.* 44, 651–653 (1984)
7. A. Lewis et al., Development of a 500 Å Resolution Light Microscope. *Ultramicroscopy* 13, 227–231 (1984)
8. J.B. Pendry, Negative refraction makes a perfect lens. *Phys. Rev. Lett.* 85(18), 3966–3969 (2000)
9. Z. Liu et al., Far-field optical hyperlens magnifying sub-diffraction-limited objects. *Science* 315(5819), 1686 (2007)
10. I.I. Smolyaninov, Y.-J. Hung, C.C. Davis, Magnifying superlens in the visible frequency range. *Science* 315(5819), 1699–1701 (2007)
11. V.A. Podolskiy, E.E. Narimanov, Near-sighted superlens. *Opt. Lett.* 30, 75–78 (2005)
12. G. Toraldo di Francia, Supergain antennas and optical resolving power. *Nuovo Cimento Suppl.* 9, 426–435 (1952)
13. W. Lukosz, Optical systems with resolving powers exceeding the classical limit. *J. Opt. Soc. Am.* 56, 1463–1472 (1966)
14. C. Cremer, T. Cremer, Considerations on a laser-scanning-microscope with high resolution and depth of field. *Microscopica Acta* 81(1), 31–44 (1978)
15. M. Minsky, *Microscopy Apparatus*. US Patent, 3,013,467 (1961)
16. T. Wilson, C.J.R. Sheppard, *Theory and Practice of Scanning Optical Microscopy* (Academic, New York, 1984)
17. J.B. Pawley, *Handbook of Biological Confocal Microscopy*, 2nd edn. (Springer, New York, 2006), p. 700
18. N. Bloembergen, *Nonlinear Optics* (Benjamin, New York, 1965)
19. C.J.R. Sheppard, R. Kompfner, Resonant scanning optical microscope. *Appl. Optics* 17, 2879–2882 (1978)
20. W. Denk, J.H. Strickler, W.W. Webb, Two-photon laser scanning fluorescence microscopy. *Science* 248, 73–76 (1990)
21. A. Schönle, S.W. Hell, Far-field fluorescence microscopy with repetitive excitation. *Eur. Phys. J. D* 6, 283–290 (1999)
22. M. Bertero, et al., Three-dimensional image restoration and super-resolution in fluorescence confocal microscopy. *J. Microsc.* 157, 3–20 (1990)
23. J.-A. Conchello, J.G. McNally, Fast regularization technique for expectation maximization algorithm for optical sectioning microscopy. *SPIE Proc.* 2655, 199–208 (1996)
24. D.H. Burns et al., Strategies for attaining superresolution using spectroscopic data as constraints. *Appl. Optics* 24(2), 154–160 (1985)

25. D.W. Pohl, D. Courjon, *Near Field Optics* (Kluwer, Dordrecht, 1993)
26. D.W. Pohl, Near-field optics: comeback of light in microscopy. *Solid State Phenom.* 63–64, 252–256 (1998)
27. E. Betzig et al., Near-field fluorescence imaging of cytoskeletal actin. *Bioimaging* 1, 129–136 (1993)
28. A. Kirsch, C. Meyer, T.M. Jovin, Integrating of optical techniques in scanning probe microscopes; The scanning near-field optical microscope (SNOM), in *Analytical Use of Fluorescent Probes in Oncology*, ed. by E. Kohen, J.G. Hirschberg (Plenum, New York, 1996), pp. 317–323
29. L. Novotny, B. Hecht, *Principles of Nano-Optics* (Cambridge University Press, Cambridge, MA, 2006)
30. R.Y. Tsien, The green fluorescent protein. *Annu. Rev. Biochem.* 67(1), pp. 509–544 (1998)
31. R.Y. Tsien, Imagining imaging's future. *Nat. Cell Biol.* 5, SS16–SS21 (2003)
32. S.W. Hell, Double-Scanning Confocal Microscope. European Patent, 0491289 (1990/1992)
33. S. Hell, E.H.K. Stelzer, Fundamental improvement of resolution with a 4Pi-confocal fluorescence microscope using two-photon excitation. *Opt. Commun.* 93, 277–282 (1992)
34. S.W. Hell, Improvement of lateral resolution in far-field light microscopy using two-photon excitation with offset beams. *Opt. Commun.* 106, 19–24 (1994)
35. S.W. Hell, J. Wichmann, Breaking the diffraction resolution limit by stimulated emission: stimulated emission depletion fluorescence microscopy. *Opt. Lett.* 19(11), 780–782 (1994)
36. S.W. Hell, M. Kroug, Ground-state depletion fluorescence microscopy: a concept for breaking the diffraction resolution limit. *Appl. Phys. B* 60, 495–497 (1995)
37. A. Schönle, P.E. Hänninen, S.W. Hell, Nonlinear fluorescence through intermolecular energy transfer and resolution increase in fluorescence microscopy. *Ann. Phys. (Leipzig)*, 8(2), 115–133 (1999)
38. S.W. Hell, S. Jakobs, L. Kastrop, Imaging and writing at the nanoscale with focused visible light through saturable optical transitions. *Appl. Phys. A* 77, 859–860 (2003)
39. S.W. Hell, Toward fluorescence nanoscopy. *Nature Biotechnol.* 21(11), 1347–1355 (2003)
40. S.W. Hell, M. Dyba, S. Jakobs, Concepts for nanoscale resolution in fluorescence microscopy. *Curr. Opin. Neurobiol.* 14(5), 599–609 (2004)
41. S.W. Hell, Strategy for far-field optical imaging and writing without diffraction limit. *Phys. Lett. A* 326(1–2), 140–145 (2004)
42. M. Hofmann et al., Breaking the diffraction barrier in fluorescence microscopy at low light intensities by using reversibly photoswitchable proteins. *Proc. Natl. Acad. Sci. USA* 102(49), 17565–17569 (2005)
43. E. Betzig et al., Imaging intracellular fluorescent proteins at nanometer resolution. *Science* 313(5793), 1642–1645 (2006)
44. M.J. Rust, M. Bates, X. Zhuang, Sub-diffraction-limit imaging by stochastic optical reconstruction microscopy (STORM). *Nat. Meth.* 3, 793–796 (2006)
45. S.T. Hess, T.P.K. Girirajan, M.D. Mason, Ultra-high resolution imaging by fluorescence photoactivation localization microscopy. *Biophys. J.* 91(11), 4258–4272 (2006)

46. S. Hell, E.H.K. Stelzer, Properties of a 4Pi-confocal fluorescence microscope. *J. Opt. Soc. Am. A* 9, 2159–2166 (1992)
47. M.G.L. Gustafsson, D.A. Agard, J.W. Sedat, Sevenfold improvement of axial resolution in 3D widefield microscopy using two objective lenses. *Proc. SPIE* 2412, 147–156 (1995)
48. M. Schrader, S.W. Hell, 4Pi-confocal images with axial superresolution. *J. Microsc.* 183, 189–193 (1996)
49. M. Nagorni, S.W. Hell, Coherent use of opposing lenses for axial resolution increase in fluorescence microscopy. I. Comparative study of concepts. *J. Opt. Soc. Am. A* 18(1), 36–48 (2001)
50. P.E. Hänninen et al., Two-photon excitation 4Pi confocal microscope: Enhanced axial resolution microscope for biological research. *Appl. Phys. Lett.* 66, 1698–1700 (1995)
51. S.W. Hell, M. Schrader, H.T.M. van der Voort, Far-field fluorescence microscopy with three-dimensional resolution in the 100 nm range. *J. Microsc.* 185(1), 1–5 (1997)
52. M. Schrader et al., 4Pi-confocal imaging in fixed biological specimens. *Biophys. J.* 75, 1659–1668 (1998)
53. M. Nagorni, S.W. Hell, 4Pi-confocal microscopy provides three-dimensional images of the microtubule network with 100- to 150-nm resolution. *J. Struct. Biol.* 123, 236–247 (1998)
54. A. Egner, S. Jakobs, S.W. Hell, Fast 100-nm resolution 3D-microscope reveals structural plasticity of mitochondria in live yeast. *Proc. Nat. Acad. Sci. U.S.A.* 99, 3370–3375 (2002)
55. A. Egner et al., 4Pi-microscopy of the Golgi apparatus in live mammalian cells. *J. Struct. Biol.* 147(1), 70–76 (2004)
56. H. Gugel et al., Cooperative 4Pi excitation and detection yields 7-fold sharper optical sections in live cell microscopy. *Biophys. J.* 87, 4146–4152 (2004)
57. J. Bewersdorf, B.T. Bennett, K.L. Knight, H2AX chromatin structures and their response to DNA damage revealed by 4Pi microscopy. *Proc. Natl. Acad. Sci. USA* 103, 18137–18142 (2006)
58. A. Egner, S.W. Hell, Fluorescence microscopy with super-resolved optical sections. *Trends Cell Biol.* 15(4), 207–215 (2005)
59. M. Lang et al., 4Pi microscopy of type A with 1-photon excitation in biological fluorescence imaging. *Opt. Expr.* 15(5), 2459–2467 (2007)
60. M. Lang, J. Engelhardt, S.W. Hell, 4Pi microscopy with linear fluorescence excitation. *Opt. Lett.* 32(3), 259–261 (2007)
61. M.C. Lang et al., 4Pi microscopy with negligible sidelobes. *New J. Phys.* 10, 1–13 (2008)
62. M.G. Gustafsson, D.A. Agard, J.W. Sedat. 3D widefield microscopy with two objective lenses: experimental verification of improved axial resolution, in *Three-Dimensional Microscopy: Image Acquisition and Processing III*, Proceedings of SPIE, 1996
63. M.G.L. Gustafsson, D.A. Agard, J.W. Sedat, I⁵M: 3D widefield light microscopy with better than 100 nm axial resolution. *J. Microsc.* 195, 10–16 (1999)
64. B. Bailey et al., Enhancement of axial resolution in fluorescence microscopy by standing-wave excitation. *Nature* 366, 44–48 (1993)
65. R. Freimann, S. Pentz, H. Hörler, Development of a standing-wave fluorescence microscope with high nodal plane flatness. *J. Microsc.* 187(3), 193–200 (1997)

66. M. Nagorni, S.W. Hell, Coherent use of opposing lenses for axial resolution increase in fluorescence microscopy. II. Power and limitation of nonlinear image restoration. *J. Opt. Soc. Am. A* 18(1), 49–54 (2001)
67. J. Bewersdorf, R. Schmidt, S.W. Hell, Comparison of I⁵M and 4Pi-microscopy. *J. Microsc.* 222, 105–117 (2006)
68. S.W. Hell, Far-field optical nanoscopy. *Science* 316(5828), 1153–1158 (2007)
69. V. Westphal, S.W. Hell, Nanoscale resolution in the focal plane of an optical microscope. *Phys. Rev. Lett.* 94, 143903 (2005)
70. B. Harke et al., Resolution scaling in STED microscopy. *Opt. Expr.* 16(6), 4154–4162 (2008)
71. R. Heintzmann, T.M. Jovin, C. Cremer, Saturated patterned excitation microscopy – A concept for optical resolution improvement. *J. Opt. Soc. Am. A* 19(8), 1599–1609 (2002)
72. M.G.L. Gustafsson, Nonlinear structured-illumination microscopy: Wide-field fluorescence imaging with theoretically unlimited resolution. *Proc. Nat. Acad. Sci. U.S.A* 102(37), 13081–13086 (2005)
73. S.W. Hell, A. Schönle, Nanoscale resolution in far-field fluorescence microscopy, in *Science of Microscopy*, S.J.C.H., ed. by P.W. Hawkes (Springer, New York, 2007), p. 790–834
74. C. Eggeling et al., Direct observation of the nanoscale dynamics of membrane lipids in a living cell. *Nature*, 457, 1159–1163 (2009)
75. S.W. Hell, Increasing the resolution of far-field fluorescence light microscopy by point-spread-function engineering, in *Topics in Fluorescence Spectroscopy*, ed. by J.R. Lakowicz (Plenum, New York, 1997), p. 361–422
76. T.A. Klar, S.W. Hell, Subdiffraction resolution in far-field fluorescence microscopy. *Opt. Lett.* 24(14), 954–956 (1999)
77. T.A. Klar et al., Fluorescence microscopy with diffraction resolution limit broken by stimulated emission. *Proc. Natl. Acad. Sci. U.S.A* 97, 8206–8210 (2000)
78. T.A. Klar, E. Engel, S.W. Hell, Breaking Abbe’s diffraction resolution limit in fluorescence microscopy with stimulated emission depletion beams of various shapes. *Phys. Rev. E* 64, 066613, 1–9 (2001)
79. W. Denk, Two-photon excitation in functional biological imaging. *J. Biomed. Opt.* 1, 296–304 (1996)
80. K.I. Willig et al., STED microscopy with continuous wave beams. *Nat. Meth.* 4(11), 915–918 (2007)
81. V. Westphal, L. Kastrup, S.W. Hell, Lateral resolution of 28 nm ($\lambda/25$) in far-field fluorescence microscopy. *Appl. Phys. B* 77(4), 377–380 (2003)
82. F. Meinecke, Stimulierte Emission im Fluoreszenzmikroskop: Das STED Konzept zur Überwindung der Abbeschen Beugungsgrenze (Diplomarbeit, Ruprecht Karls Universität, Heidelberg, 1996)
83. M. Dyba, S.W. Hell, Focal spots of size $\lambda/23$ open up far-field fluorescence microscopy at 33 nm axial resolution. *Phys. Rev. Lett.* 88, 163901 (2002)
84. M. Dyba, S. Jakobs, S.W. Hell, Immunofluorescence stimulated emission depletion microscopy. *Nat. Biotechnol.* 21(11), 1303–1304 (2003)
85. G. Donnert et al., Macromolecular-scale resolution in biological fluorescence microscopy. *Proc. Natl. Acad. Sci. USA* 103(31), 11440–11445 (2006)
86. D. Wildanger et al., STED microscopy with a supercontinuum laser source. *Opt. Expr.* 16(13), 9614–9621 (2008)
87. R. Schmidt et al., Spherical nanosized spot unravels the interior of cells. *Nat. Meth.* 4(1), 81–86 (2008)

88. J. Keller, A. Schönle, S.W. Hell, Efficient fluorescence inhibition patterns for RESOLFT microscopy. *Opt. Express* 15(6), 3361–3371 (2007)
89. K.I. Willig et al., STED-microscopy reveals that synaptotagmin remains clustered after synaptic vesicle exocytosis. *Nature* 440(7086), 935–939 (2006)
90. R.J. Kittel et al., Bruchpilot promotes active zone assembly, Ca²⁺-channel clustering, and vesicle release. *Science* 312, 1051–1054 (2006)
91. J.J. Sieber et al., The SNARE motif is essential for the formation of syntaxin clusters in the plasma membrane. *Biophys. J.* 90, 2843–2851 (2006)
92. R. Kellner et al., Nanoscale organization of nicotinic acetylcholine receptors revealed by STED microscopy. *Neuroscience* 144(1), 135–143 (2007)
93. V. Westphal et al., Dynamic far-field fluorescence nanoscopy. *New J. Phys.* 9, 435 (2007)
94. V. Westphal et al., Video-rate far-field optical nanoscopy dissects synaptic vesicle movement. *Science* 320(5873), 246–249 (2008)
95. L. Kastrup et al., Fluorescence fluctuation spectroscopy in subdiffraction focal volumes. *Phys. Rev. Lett.* 94, 178104 (2005)
96. B. Hein, K. Willig, S.W. Hell, Stimulated emission depletion (STED) nanoscopy of a fluorescent protein – labeled organelle inside a living cell. *Proc. Natl. Acad. Sci. U S A* 105(38), 14271–14276 (2008)
97. V.U. Nägerl et al., Live-cell imaging of dendritic spines by STED microscopy. *Proc. Natl. Acad. Sci. USA* 105(48), 18982–18987 (2008)
98. K. Willig et al., STED microscopy resolves nanoparticle assemblies. *New J. Phys.* 8, 106 (2006)
99. B. Harke et al., Three-dimensional nanoscopy of colloidal crystals. *Nano Lett.* 8(5), 1309–1313 (2008)
100. E. Rittweger et al., STED microscopy reveals color centers with nanometric resolution. *Nat. Photonics*, 3, 144–147 (2009).
101. G. Balasubramanian et al., Nanoscale imaging magnetometry with diamond spins under ambient conditions. *Nature* 455, 648–651 (2008)
102. J.R. Maze et al., Nanoscale magnetic sensing with an individual electronic spin in diamond. *Nature* 455, 644–647 (2008)
103. C.C. Fu et al., Characterization and application of single fluorescent nanodiamonds as cellular biomarkers. *Proc. Nat. Acad. Sci. U.S.A.* 104(3), 727–732 (2007)
104. J.I. Chao et al., Nanometer-sized diamond particle as a probe for biolabeling. *Biophys. J.* 93(6), 2199–2208 (2007)
105. S. Bretschneider, C. Eggeling, S.W. Hell, Breaking the diffraction barrier in fluorescence microscopy by optical shelving. *Phys. Rev. Lett.* 98, 218103 (2007)
106. K.A. Lukyanov et al., Natural animal coloration can be determined by a nonfluorescent green fluorescent protein homolog. *J. Biol. Chem.* 275(34), 25879–25882 (2000)
107. R. Ando, H. Mizuno, A. Miyawaki, Regulated fast nucleocytoplasmic shuttling observed by reversible protein highlighting. *Science*. 306(5700), 1370–1373 (2004)
108. O. Haerberle, Kindling molecules: a new way to ‘break’ the Abbe limit. *C.R. Physique* 5, 143–148 (2004)
109. W. Heisenberg, *The Physical Principles of the Quantum Theory* (Chicago University Press, Chicago, 1930)
110. N. Bobroff, Position measurement with a resolution and noise-limited instrument. *Rev. Sci. Instrum.* 57(6), 1152–1157 (1986)

111. M.P. Gordon, T. Ha, P.R. Selvin, Single-molecule high-resolution imaging with photobleaching. *Proc. Natl. Acad. Sci. U S A* 101, 6462–6465 (2004)
112. X. Qu et al., Nanometer-localized multiple single-molecule fluorescence microscopy. *Proc. Natl. Acad. Sci. USA* 101(31), 11298–11303 (2004)
113. H.F. Hess, E. Betzig, Optical microscopy with phototransformable labels. Patent Appl, WO 2006/127692 A2 (2005/2006)
114. S.W. Hell, Verfahren und Fluoreszenzlichtmikroskop zum räumlich hochauflösenden Abbilden einer Struktur einer Probe. German Patent, **DE 10 2006 021 317** (2006/2007)
115. M. Bates et al., Multicolor super-resolution imaging with photo-switchable fluorescent probes. *Science* 317, 1749–1753 (2007)
116. J. Fölling et al., Photochromic rhodamines provide nanoscopy with optical sectioning. *Angew. Chem. Int. Ed.* 46, 6266–6270 (2007)
117. H. Bock et al., Two-color far-field fluorescence nanoscopy based on photo-switching emitters. *Appl. Phys. B* 88, 161–165 (2007)
118. C. Geisler et al., Resolution of $\lambda/10$ in fluorescence microscopy using fast single molecule photo-switching. *Appl. Phys. A* 88(2), 223–226 (2007)
119. A. Egner et al., Fluorescence nanoscopy in whole cells by asynchronous localization of photoswitching emitters. *Biophys. J.* 93, 3285–3290 (2007)
120. B. Huang et al., Three-dimensional super-resolution imaging by stochastic optical reconstruction microscopy. *Science* 319, 810–813 (2008)
121. H. Shroff et al., Live-cell photoactivated localization microscopy of nanoscale adhesion dynamics. *Nat. Meth.* 5(5), 417–423 (2008)
122. H. Shroff et al., Dual-color superresolution imaging of genetically expressed probes within individual adhesion complexes. *Proc. Natl. Acad. Sci. U.S.A.* 104(51), 20308–20313 (2007)
123. J. Fölling et al., Fluorescence nanoscopy by ground-state depletion and single-molecule return. *Nat. Meth.* 5, 943–945 (2008)
124. M. Bossi et al., Multi-color far-field fluorescence nanoscopy through isolated detection of distinct molecular species. *Nano Lett.* 8(8), 2463–2468 (2008)
125. S. Weiss, Fluorescence spectroscopy of single biomolecules. *Science* 283, 1676–1683 (1999)
126. A. Yildiz et al., Myosin V walks hand-over-hand: single fluorophore imaging with 1.5-nm localization. *Science* 300(5628), 2061–2065 (2003)
127. A.M. van Oijen et al., Far-field fluorescence microscopy beyond the diffraction limit. *J. Opt. Soc. Am. A* 16(4), 909–915 (1999)
128. E. Betzig, Proposed method for molecular optical imaging. *Opt. Lett.* 20(3), 237–239 (1995)
129. K.A. Lidke et al., Superresolution by localization of quantum dots using blinking statistics. *Opt. Expr.* 13(18), 7052–7062 (2005)
130. S.W. Hell, J. Soukka, P.E. Hänninen, Two- and multiphoton detection as an imaging mode and means of increasing the resolution in far-field light microscopy. *Bioimaging* 3, 65–69 (1995)
131. J. Fölling et al., Fluorescence nanoscopy with optical sectioning by two-photon induced molecular switching using continuous-wave lasers. *Chem. Phys. Chem.* 9, 321–326 (2008)
132. M.F. Juette et al., Three-dimensional sub-100 nm resolution fluorescence microscopy of thick samples. *Nat. Meth.* 5(6), 527–529 (2008)
133. C.v. Middendorff et al., Isotropic 3D Nanoscopy based on single emitter switching. *Opt. Expr.* 16(25), 20774–20788 (2008)